Karlsruhe Institute of Technology

FAKULTÄT FÜR PHYSIK
Praktikum Moderne Physik

Praktikum: P4 Gruppe: 22 ■ Mo □ Mi **WS20/21**

Zutreffendes bitte ausfüllen

Namen: Paul Filip useba[at]student.kit.edu

Namen: Janic Beck

Versuch: MOKE

Betreuer: Daria Gusenkova Durchgeführt am: 14.12.202

Wird vom Betreuer ausgefüllt.

1. Abgabe am: _____

Rückgabe am: _____ Kommentar:

2. Abgabe am: _____

Ergebnis: + / 0 / - Handzeichen: _____

Datum: _____ Kommentar:

Contents

1. Theory & Preparation

1.1 Aim of the Experiment

In the experiment, the magnetization curves of different magnetic materials are determined. The **magneto-optical Kerr effect (MOKE)** is used. In this effect, the linearly polarized light reflected from the magnetic material undergoes a rotation of the plane of polarization. The angle of rotation Φ_K can therefore be used to draw conclusions about the magnetization. For this purpose, different layer systems consisting of ferro-, anti-ferro- and ferrimagnetic components are used.

1.2 Polarisation

The polarization of an electromagnetic wave describes the direction of oscillation of the component of the electric field in relation to the direction of propagation. A distinction is made between linear, circular and elliptical polarization. By superposition of a right circular polarized $\vec{E}^-$- and a left circular polarized $\vec{E}^+$-wave a linear polarized wave can be represented. For a circularly polarized wave, the magnitude of the electric field $|\vec{E}|$ is constant, but its direction rotates at a constant rate in the polarization plane.

$$\vec{E}_0 = \vec{E}^+ + \vec{E}^- \qquad \text{with:} \qquad E^\pm = \frac{E_0}{2} \begin{pmatrix} 1 \\ \pm i \\ 0 \end{pmatrix} \tag{1.1}$$

1.3 Magnetic field in matter

Due to atomic magnetic dipole moments, materials possess magnetic properties. The sum of all atomic magnetic moments $\vec{m}_i$ divided by the volume gives the magnetization:

$$\vec{M} = \frac{\vec{m}}{V}. \tag{1.2}$$

Thus, the magnetic flux density can be determined to:

$$\vec{B} = \mu_0 \vec{H} + \mu_0 \vec{M} = \mu_0 \mu \vec{H} \qquad with: \qquad \mu = 1 + \chi_m. \tag{1.3}$$

Here χ_m is equal to the magnetic susceptibility.

1.4 Magneto-optical Kerr effect

The **MOKE** changes the direction of polarization and intensity of the light beam reflected from a magnetic layer system. The effect results from the side diagonal elements of the permittivity tensor ϵ. This results in an anisotropic permitivity and finally in a direction dependent phase velocity in the medium with:

$$v_p = \frac{c}{\sqrt{\epsilon_r \mu_r}}. \tag{1.4}$$

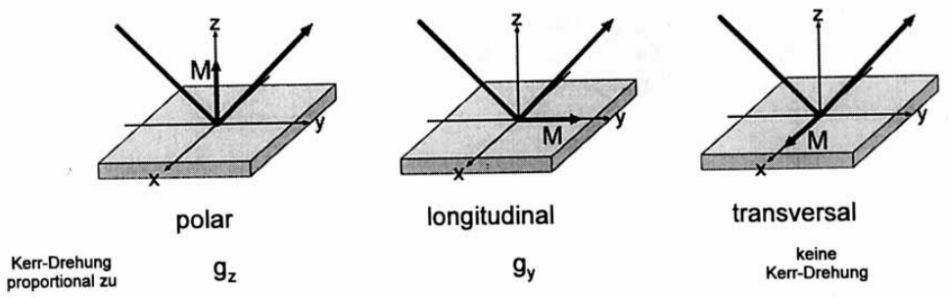

Figure 1.1: Ilustration of MOKE with different geometries

Different geometries can now be distinguished, the magnitude of the effect typically decreases by one order in each case. The **polar** MOKE occurs when magnetization is perpendicular to the surface, this has the greatest influence. Furthermore, the **longitudinal** MOKE occurs when the magnetization is oriented parallel to the surface and to the plane of incidence of light. Lastly, the **transversal** MOKE occurs when the magnetization is parallel to the surface but perpendicular to the optical plane.

We consider for simplicity a perpendicular incident beam, the refractive index of a circularly polarized wave can thus be determined by:

$$\vec{n}^{\pm} \approx \vec{n}_0 \left(1 \pm \frac{\hat{n}_0 \cdot \vec{g}}{2}\right). \tag{1.5}$$

Where $\hat{n}_0$ is the unit vector parallel to the propagation direction ($\hat{k}$) and $\vec{g}$ is the gyration vector with $Q = |\vec{g}|$ being the Voigt constant. It follows that with $\vec{g} \parallel \hat{n}_0$ for the reflection coefficient:

$$r^{\pm} = \frac{n_0 \cdot (1 \pm 0.5 \cdot Q)) - 1}{n_0 \cdot (1 \pm 0.5 \cdot Q)) + 1} \tag{1.6}$$

Choosing an incident EM wave parallel to the x-axis and the magnetization in the z-direction, i.e., the surface in the x-y plane, it follows:

$$\vec{E}i = \frac{E_0}{2}\left[\begin{pmatrix} 1 \\ i \\ 0 \end{pmatrix} + \begin{pmatrix} 1 \\ -i \\ 0 \end{pmatrix}\right] \tag{1.7}$$

$$\vec{E}^r = r^+\vec{E}^{i,+} + r^-\vec{E}^{i,-} = \left(E_0 \frac{n_0 - 1}{n_0 + 1} \cdot \vec{e}_x + \frac{n_0 \cdot Q}{(n_0 + 1)^2} \cdot i\vec{e}_y\right) \tag{1.8}$$

Here terms proportional to Q^2 were neglected. One recognizes a y-component of the reflected electric field as a result from the Kerr effect. The complex Kerr angle is then given by:

$$\Phi_K = \frac{E_y^r}{E_x^r} = i n_0 Q \frac{1}{n_0^2 - 1} \tag{1.9}$$

Considering a purely real n_0, there is no rotation of the plane of polarization. The Kerr angle corresponds to the phase shift of the two waves. The reflected wave is therefore elliptically polarized. For a complex n_0 one obtains a real Kerr angle and thus an additional change of the plane of polarization.

1.5 Magnetic anisotropy

Magnetic anisotropy describes a preferred direction in the magnetization of a material. It is described by the magnetic anisotropy energy, the work required to rotate the magnetization

$\vec{M}$ out of the easy direction in a closed system without particle exchange. The easy direction corresponds to the energetically preferred direction of spontaneous magnetization. The microscopic cause of the magnetic anisotropy is the dipole-dipole interaction and the spin-orbit coupling.
By a thermodynamic consideration, one can determine the Gibbs free energy by:

$$F = -J_S H \cos(\Theta - \Theta_H) + K_{eff} \sin^2(\Theta) \qquad \text{with:} \qquad J_S = \mu_0 M_S \tag{1.10}$$

Where:

- M_S: magnetic polarization
- M_S: Saturation magnetization
- H: magnitude of the applied magnetic field
- Θ_H: Angle between the surface normal and the magnetic field
- Θ: Angle between the surface normal and the magnetization
- K_{eff}: the effective anisotropy constant

Here, the anisotropy constant is given by:

$$K_{eff} = -\frac{J_s^2}{2\mu_0} + K_1 + \frac{2k_s}{d}, \tag{1.11}$$

the terms are describing the shape anisotropy, magnetocrisstalline anisotropy of hexagonal symmetry and the interface anisotropy. K_{eff} corresponds to the area under the magnetization curve.
The free energy is a thermodynamic potential and tends to a minimum at thermodynamic equilibrium. In polar MOKE, $\Theta_H = 0$ holds, thus the anisotropy constant can be determined by the equilibrium condition when the material reaches saturation.

$$\frac{dF}{d\Theta} = 0 \tag{1.12}$$

$$\Rightarrow K_{eff} = -\frac{1}{2}\mu_0 M_S H = -\frac{1}{2} J_S \tag{1.13}$$

By measuring the hysteresis curve, the coercivity H_C must still be subtracted from the saturation field strength H_S. In addition, the kerr angle Φ_S in the saturation region is proportional to the saturation magnetization.

$$J_S \propto \Phi_S \tag{1.14}$$

Thus we can calculate the effective anisotropy constant to:

$$K_{eff} \propto -\frac{1}{2}\Phi_S (H_S - H_C) \tag{1.15}$$

1.6 Relevant types of magnetism

1.6.1 Ferromagnetism

1.6.2 Anti ferromagnetism

1.6.3 Ferrimagnetism

2. Experiment & Evaluation

2.1 Experimental setup

As can be seen in Figure **??**, a sample can be placed inside of an electromagnet with controllable B-field. The measurement apparatus that will test the magneto-optic Kerr effect consists of a laser diode that shines polarised light onto the sample. Two polarisation filters and focusing lenses exist to tweak the properties of light beam and improve the overall signal strength. The light that gets reflected off the magnetic sample travels trough a beam splitter into two photo diodes that in turn feed a differential amplifier. A Hall probe monitors the strength of the B-field in which the sample is placed.

2.2 Ferromagnets: Pd/Co/Pd sample

The first sample consists of two thin layers of Palladium (paramagnetic) and one layer of Cobalt (ferromagnetic) of variable thickness (0.3 nm - 2 nm) labelled in the following as d. The crystal lattice of the trilayer system in total acts as a ferromagnet. The different magnetic properties of the sublattice however can cause strong changes in both magnitude and direction of magnetization in special cases. These effects will in part be analysed in this section.

Before the measurement data is evaluated the applied model is presented. The Kerr-angle that is measured as a function of external magnetic field is proportional to the magnetic induction. We are therefore effectively measuring a magnetic hysteresis modulo some numerical constants. Expanding on the work in [Tak01] we can therefore impose a model to analytically describe the hysteresis curve traced out by the Kerr-angle Φ in varying magnetic fields. This model is presented in Equation 2.1.

$$\Phi(H) = \Phi_s \tanh\left(A(H \pm H_c)\right) + \mu H. \tag{2.1}$$

Here introduced are several parameters that influence the shape of the hysteresis curve.

- Φ_s is the Kerr-angle at the saturation point.
- A[1] determines the magnetic hardness of the sample.
- $\pm H_c$ is the coercive field strength, on the up/downsweep of H.
- μ is the magnetic permeability of air.

The last term ($+\mu H$) in Equation 2.1 stems from the definition of magnetic induction ($\vec{B} = \mu(\vec{M} + \vec{H})$). In theory, it should be possible to extract information about the magnetic permeability from the best fit value of μ. In practice, effects caused for example

[1] for lack of more fitting nomenclature in the literature

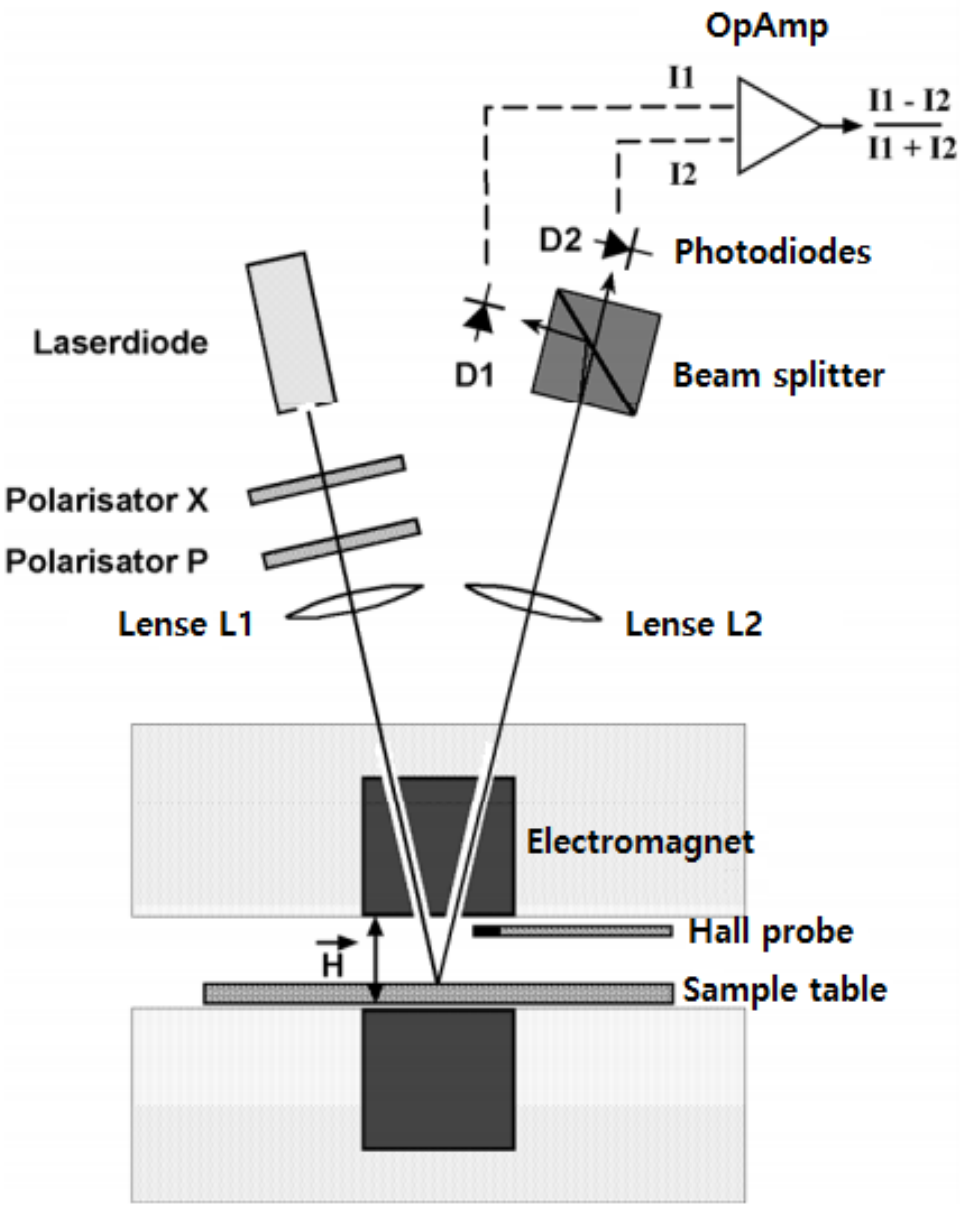

Figure 2.1
Experimental setup of the MOKE lab, image adopted with changes from [Unk08]

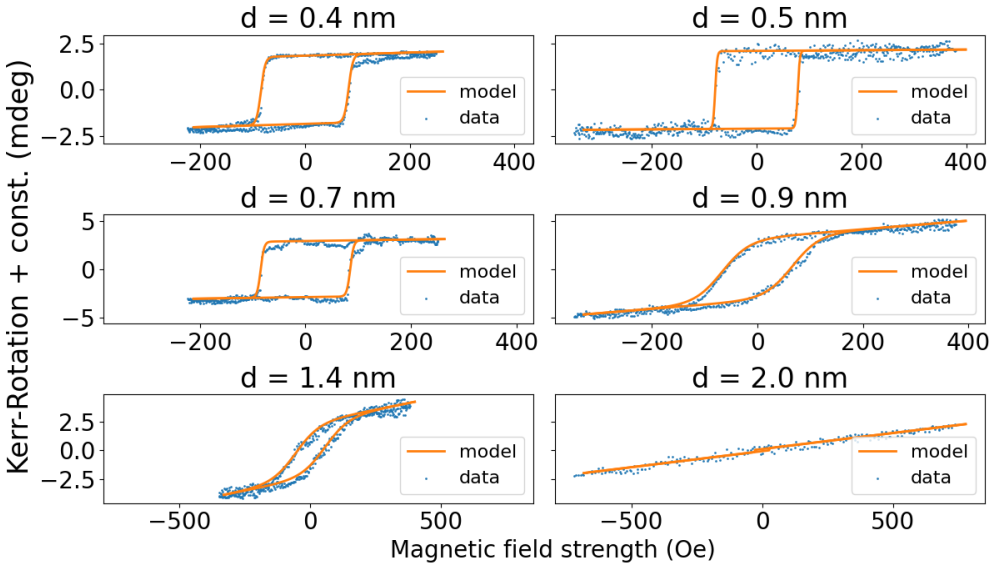

Figure 2.2: The hysteresis of a Pd/Co/Pd layer system for different Co-layer thicknesses.

by the layering of different magnetic materials make a prediction rather difficult. For the purpose of the following analysis, the exact value of μ is not important anyways.

Once the measurements of the Kerr-angle in relation to external magnetic field are taken, the set of Kerr-angles is offset by its mean value. This eliminates systematic errors in the data and helps to compare measurement values across the different measurement sets varying in Co-layer thickness d. This is the only correction applied to the dataset and is sufficient to make qualitative statements about the magnetic properties of the sample. The results of the analysis are presented in Figure 2.2 and Table 2.1.

At first glance, the results seem intuitive. For layer thicknesses of 0.4 nm to 0.9 nm the magnetic properties such as coercive field strength or hardness of the material agree within an order of magnitude. Regarding the imperfections in both measurement apparatus and applied model, this implies the magnetic properties do not change. Only the Kerr-angle at saturation, Φ_s, seems to display an upwards trend with increasing d. This is expected, since a thicker layer allows for more domains to become magnetised, causing a higher net magnetisation (and by extension Kerr-angle) at a given external magnetic field H.

The magnetic behaviour for thicker Co-layers drastically changes. As explained in the lab manual, this is most likely caused by anisotropic effects near the boundaries of the different magnetic layers. For certain values of d, the magnetisation seems to point into the transversal direction of of the measurement plane (compare Figure 1.1). Under such circumstances, the magneto-optic Kerr effect disappears and a hysteresis is no longer visible. This culminates in unphysical fit parameters for a Co-layer thickness of 2.0 nm, where the fitting algorithm attempts to fit a hysteresis to a dataset that does not display any such behaviour and is purely dominated by the last term in Equation 2.1. For smaller layer thicknesses (1.4 nm and 1.7 nm) this effect can already be observed in parts.

The effective anisotropy constant K_{eff} helps quantifying the strength of these boundary layer effects. The values of K_{eff} for different Co-layer thicknesses are give in Table 2.2.

Table 2.1: Hysteresis best fit values for different Co-layer thicknesses. Statistical errors estimated by the fitting algorithm are neglected due to their relative size being about 10^{-5}. This does not accurately represent the true uncertainty of the dataset.

d	Φ_s	A	H_c	μ
0.4 nm	1.84 mdeg	121.3604 $\frac{1}{\text{mOe}}$	83.59 Oe	0.84 $\frac{\mu\text{deg}}{\text{Oe}}$
0.5 nm	2.10 mdeg	260.5127 $\frac{1}{\text{mOe}}$	78.79 Oe	0.18 $\frac{\mu\text{deg}}{\text{Oe}}$
0.7 nm	2.91 mdeg	152.2159 $\frac{1}{\text{mOe}}$	84.84 Oe	0.77 $\frac{\mu\text{deg}}{\text{Oe}}$
0.9 nm	3.24 mdeg	19.1988 $\frac{1}{\text{mOe}}$	66.67 Oe	4.44 $\frac{\mu\text{deg}}{\text{Oe}}$
1.4 nm	2.40 mdeg	10.9649 $\frac{1}{\text{mOe}}$	55.91 Oe	4.54 $\frac{\mu\text{deg}}{\text{Oe}}$
2.0 nm	0.10 mdeg	1362.8763 $\frac{1}{\text{mOe}}$	−28.30 Oe	2.79 $\frac{\mu\text{deg}}{\text{Oe}}$

Table 2.2: Effective anisotropy constant in relation to Co-layer thickness

d	Φ_s	H_s	H_c	$K_{\text{eff}} = -\frac{1}{2}\Phi_s(H_s - H_c)$
0.4 nm	1.84 mdeg	99.07 Oe	83.59 Oe	−14.25 $\frac{\text{mdeg}}{\text{Oe}}$
0.5 nm	2.10 mdeg	89.68 Oe	78.79 Oe	−11.42 $\frac{\text{mdeg}}{\text{Oe}}$
0.7 nm	2.91 mdeg	99.05 Oe	84.84 Oe	−20.67 $\frac{\text{mdeg}}{\text{Oe}}$
0.9 nm	3.24 mdeg	127.52 Oe	66.67 Oe	−98.63 $\frac{\text{mdeg}}{\text{Oe}}$
1.4 nm	2.40 mdeg	140.86 Oe	55.91 Oe	−101.89 $\frac{\text{mdeg}}{\text{Oe}}$
2.0 nm	0.10 mdeg	−0.58 Oe	−28.30 Oe	−1.33 $\frac{\text{mdeg}}{\text{Oe}}$

2.3 Antiferromagnets: Co/Pd/Co sample

2.4 Ferrimagnets: $Fe_{1-x}Gd_x$ samples

Lastly, layered systems of Iron (Fe) and Gadolinium (Gd) are tested for their magnetic properties. Several samples with varying Gd-concentrations of $x\,\%$ are available to be experimented on. Unfortunately only one of the samples (#6) delivered physically sensible data at the time of the experiment. As a consequence, only the set of measurements pertaining to this sample will be analysed in depth.

During measurements, the sample is placed on a heating module, whose temperature can be controlled by adjusting an applied voltage. Due to large fluctuations in temperature during measurements, the uneven contact of the sample to the heating element as well as other environmental factors, the temperature of the sample is assumed to have an uncertainty of $\pm 1\,°\mathrm{C}$. After the hysteresis at a specific temperature is measured, the temperature of the sample is changed and the process is repeated for a different temperature. The results of this survey are fitted to the theoretical model introduced in section 2.2. The gathered model parameters are presented in Table 2.3. A select few measurement are also visualised in Figure 2.3. As can be seen in both the table and the figure, the coercive field strength (H_c) decreases with increasing temperature. This is expected. The two antiparallel magnetic sublattices in the sample react differently to temperature. As a consequence, the net magnetisation of the sample varies throughout the measurement process. At a specific temperature $T_{\text{comp.}}$, the magnetisation of the lattices are exactly opposite, causing a net magnetisation of zero. This is best seen by plotting the coercive field strength H_c over sample temperature T, as is done in Figure 2.4. Fitting a third order polynomial to the data points reveals, that the coercive field in this remperature regime can be roughly described by Equation 2.2.

$$H_c(T) = -0.24(2)\,\frac{\mathrm{mOe}}{°\mathrm{C}^3}\,T^3 + 0.042(3)\,\frac{\mathrm{Oe}}{°\mathrm{C}^2}\,T^2 + -3.0(1)\,\frac{\mathrm{Oe}}{°\mathrm{C}}\,T + 94.6(8)\,\mathrm{Oe} \tag{2.2}$$

The compensation temperature is then given as the temperature, where the coercive field is zero. Uncertainties in this result can be approximated using a maximum error estimation with the values given in Equation 2.2.

$$T_{\text{comp.}} = 81.4^{+1.0}_{-0.9}\,°\mathrm{C}$$

Corollarily, the Gd concentration x can be estimated using the formula given in [Unk08].

$$\begin{aligned} x\,(\mathrm{at}\%) &= 0.01783\;\; T_{\text{comp.}} + 21 \\ &= 22.451^{+0.017}_{-0.016}\,\% \end{aligned}$$

The influence of compensation temperature on the Kerr-angle at saturation Φ_s remains the last unanswered question. For low temperatures, the magnetisation of the gadolinium dominates the magnetic properties of the sample, but because Gd has a low Curie-temperature than iron, it is expected that for higher temperatures the magnetisation of the iron sublattice becomes relevant. Accordingly, the Kerr-angle at satureation Φ_s is expected to drop with increasing compensation temperature. This can however not be verified experimentally.

2.5 Conclusion

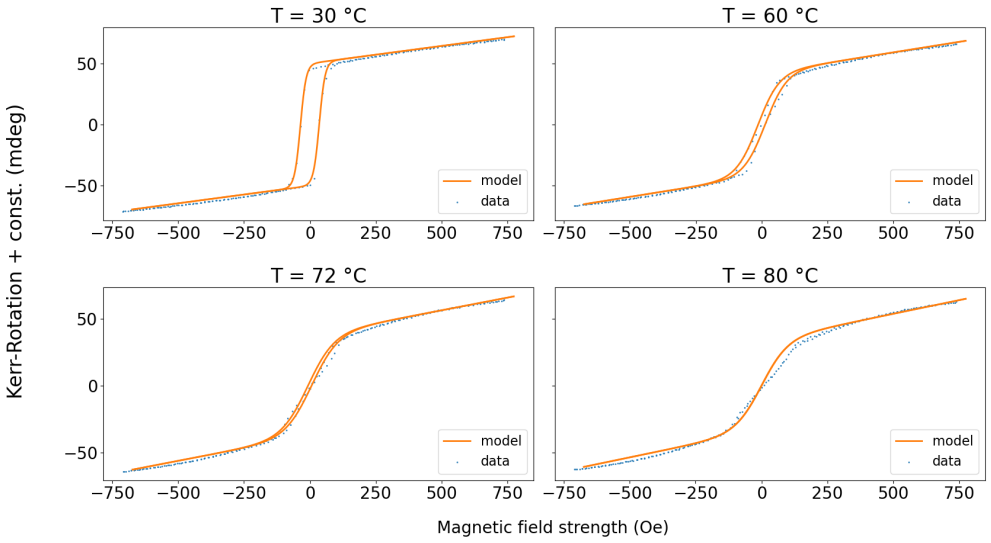

Figure 2.3: The hysteresis of a FeGd layer system for different temperatures

Table 2.3: Hysteresis best fit values for different magnet temperatures. Statistical errors estimated by the fitting algorithm are again neglected due to their small relative sizes.

T	Φ_s	A	H_c	μ
0 °C	58.6761 mdeg	149.7627 $\frac{1}{\mathrm{mOe}}$	94.93 Oe	26.36 $\frac{\mu\mathrm{deg}}{\mathrm{Oe}}$
10 °C	55.2614 mdeg	123.4514 $\frac{1}{\mathrm{mOe}}$	69.87 Oe	25.02 $\frac{\mu\mathrm{deg}}{\mathrm{Oe}}$
20 °C	53.0343 mdeg	68.1633 $\frac{1}{\mathrm{mOe}}$	50.90 Oe	26.50 $\frac{\mu\mathrm{deg}}{\mathrm{Oe}}$
30 °C	50.1260 mdeg	45.6059 $\frac{1}{\mathrm{mOe}}$	35.93 Oe	28.72 $\frac{\mu\mathrm{deg}}{\mathrm{Oe}}$
40 °C	47.5209 mdeg	26.9361 $\frac{1}{\mathrm{mOe}}$	25.27 Oe	30.24 $\frac{\mu\mathrm{deg}}{\mathrm{Oe}}$
50 °C	45.1964 mdeg	18.8061 $\frac{1}{\mathrm{mOe}}$	19.83 Oe	32.16 $\frac{\mu\mathrm{deg}}{\mathrm{Oe}}$
60 °C	41.9797 mdeg	12.2294 $\frac{1}{\mathrm{mOe}}$	14.17 Oe	34.46 $\frac{\mu\mathrm{deg}}{\mathrm{Oe}}$
70 °C	38.8206 mdeg	10.0000 $\frac{1}{\mathrm{mOe}}$	9.60 Oe	36.90 $\frac{\mu\mathrm{deg}}{\mathrm{Oe}}$
72 °C	37.3744 mdeg	10.0000 $\frac{1}{\mathrm{mOe}}$	7.47 Oe	37.96 $\frac{\mu\mathrm{deg}}{\mathrm{Oe}}$
75 °C	37.2512 mdeg	10.0000 $\frac{1}{\mathrm{mOe}}$	6.18 Oe	38.06 $\frac{\mu\mathrm{deg}}{\mathrm{Oe}}$
80 °C	33.3113 mdeg	10.0000 $\frac{1}{\mathrm{mOe}}$	−0.51 Oe	40.87 $\frac{\mu\mathrm{deg}}{\mathrm{Oe}}$

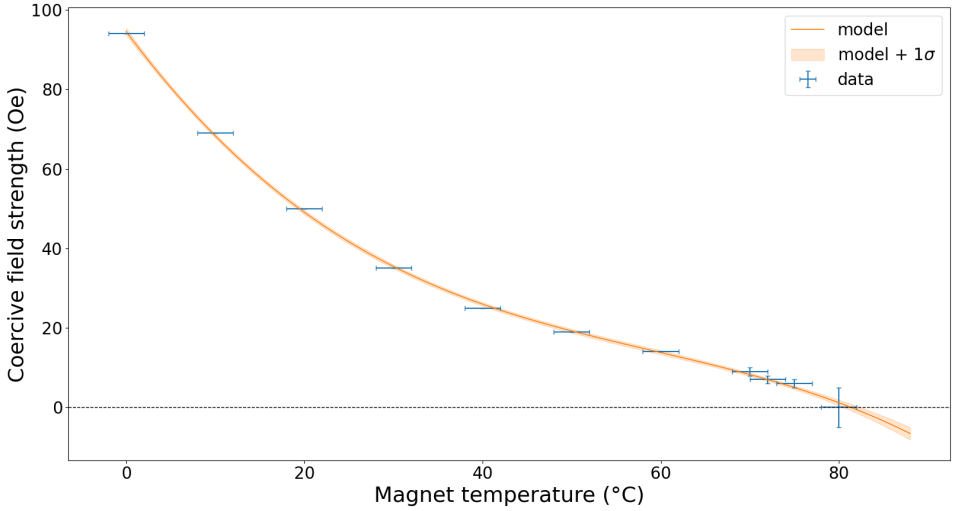

Figure 2.4: Coercive field strength of a FeGd layer system over temperature

Bibliography

[Tak01] Takács, Jenõ: *A phenomenological mathematical model of hysteresis.* Compel-the International Journal for Computation and Mathematics in Electrical and Electronic Engineering - COMPEL-INT J COMPUT MATH ELEC, 20:1002–1015, Dezember 2001.

[Unk08] Unknown: *Magnetooptischer Kerr-Effekt (MOKE).* 2008.